Journal of Computational Physics 228 (2009) 4232–4247

Contents lists available at ScienceDirect

Journal of Computational Physics

journal homepage: www.elsevier.com/locate/jcp

A characteristic-based nonconvex entropy-fix upwind scheme for the ideal magnetohydrodynamic equations ☆

Susana Serna

Department of Mathematics, University of California Los Angeles, Los Angeles, CA 90095-1555, USA

ARTICLE INFO

Article history:
Received 14 April 2008
Received in revised form 3 February 2009
Accepted 2 March 2009
Available online 11 March 2009

Dedicated to Professor Antonio Marquina on the occasion of his 60th birthday.

Keywords:
Hyperbolic conservation laws
Ideal magnetohydrodynamic equations
Local characteristic fields
Upwind schemes

ABSTRACT

In this paper we perform an analysis of the wave structure of the ideal magnetohydrodynamic (MHD) equations. We present an analytical expression of the nonlinearity term associated to each characteristic field derived from a scaled version of the complete system of eigenvectors proposed by Brio and Wu [M. Brio, C.C. Wu, An upwind differencing scheme for the equations of ideal magnetohydrodynamics, J. Comput. Phys. 75 (2) (1988) 400–422] and adopting the eight wave approach by Powell et al. [K.G. Powell, P.L. Roe, R.S. Myong, T. Gombosi, D. deZeeuw, An upwind scheme for magnetohydrodynamics, AIAA 12th Computational Fluid Dynamics Conference, San Diego, CA, 1995, pp. 661–674]. A criterion for the detection of local regions containing points for which a nonlinear characteristic field becomes nonconvex is formulated for the two-dimensional case. We then design a characteristic-based upwind scheme for the ideal MHD equations that resolves the wave dynamics by local characteristic wavefields. The new scheme is able to detect local regions containing nonconvex singularities and to handle an entropy correction through a prescription of a local viscosity ensuring convergence to the entropy solution. A third order accurate version of the scheme performs satisfactorily in resolving one and two-dimensional MHD problems. Numerical results indicate that the proposed scheme behaves low dissipative, stable and accurate under high CFL numbers.

1. Introduction

The ideal magnetohydrodynamics (MHD) system of equations can be expressed as

$$\rho_t = -\nabla(\rho\mathbf{v}), \tag{1}$$

$$(\rho\mathbf{v})_t = -\nabla\left(\rho\mathbf{v}\mathbf{v}^T + \left(P + \frac{1}{2}\mathbf{B}^2\right)I - \mathbf{B}\mathbf{B}^T\right), \tag{2}$$

$$\mathbf{B}_t = \nabla \times (\mathbf{v} \times \mathbf{B}), \tag{3}$$

$$E_t = -\nabla\left(\left(\frac{\gamma}{\gamma-1}P + \frac{1}{2}\rho q^2\right)\mathbf{v} - (\mathbf{v} \times \mathbf{B}) \times \mathbf{B}\right), \tag{4}$$

where $\rho, P, \mathbf{v}, \mathbf{B}$ and E denote the mass density, the pressure, the velocity field, the magnetic field and the total energy respectively. The adiabatic constant is represented by γ and the energy $E = \frac{1}{2}\rho q^2 + \frac{1}{2}B^2 + \frac{P}{\gamma-1}$ where q^2 and B^2 are the squares of the magnitudes of the velocity field and the magnetic field respectively. The hydrodynamic pressure is defined through the ideal gas EOS as $P = (\gamma - 1)\rho\epsilon$ where ϵ is the specific internal energy.

☆ This work is supported by Grants DGICYT MTM2008-03597 and BAA-H-M1582-07-BA001.
E-mail address: serna@math.ucla.edu

0021-9991/$ - see front matter © 2009 Elsevier Inc. All rights reserved.
doi:10.1016/j.jcp.2009.03.001

The ideal MHD wave dynamics is more complicated than the one for ideal gases. There exist hyperbolic singularities where the MHD eigensystem is not well behaved and the presence of the magnetic field generates new magnetic and magnetoacoustic waves. The rotation of the magnetic field induces non-strict hyperbolicity of the MHD system and non-genuinely nonlinearity in some of the local wavefields [4,5].

Analytical studies and numerical simulations play an important role in investigating the motion of ionized gases described by the ideal MHD equations. From the analytical perspective the standard approach is based on the study of the wave structure arising from the equations ([14,4,5,28]) and from the numerical one the strategy consists in the development of numerical schemes able to reproduce and explore the physical properties of the MHD flow ([5,15,27]).

In this research work we analyze the nonconvex wave structure of the ideal MHD system of equations and propose a numerical scheme for its approximation.

Our approach follows the recent theory of MHD shock waves based on dissipative MHD ([27]) that maintains three relevant features namely: the existence of intermediate shocks, the involvement of time-dependent intermediate shocks in the rotation of the magnetic field and the dependence of the complex wave structure on the shock dissipation mechanism.

Well behaved numerical schemes converge to the entropy solution of the system of equations ([13]). Numerical schemes for the approximation of the solution of ideal MHD equations require dissipation to be well behaved and develop the complex wave structure that appears in the dynamics as a consequence of the nonlinear wave interaction. Most numerical Godunov-type schemes for ideal MHD equations are designed to prescribe a global dissipation ([1,2,15,18]). The viscosity prescription ensures stability and computational efficiency but on the other hand the excessive dissipation implies loss of accuracy and smearing of fine structure. Different ways to overcome the excess of dissipation include the use of very fine grids or the implementation of very high order versions of the scheme.

The Godunov upwind scheme allows to achieve precise control of the numerical dissipation ([11,22]). This scheme defines, from the local characteristic structure, an upwind choice at cell interfaces as the result of the solution of the Riemann problem. Upwind schemes are defined according to the sign of the local wave velocities, propagate waves with correct speed and are featured by their low local dissipative behavior ([9,11,21,22]). However, because of the lack of dissipation, upwind schemes may fail to converge to the entropy solution around points of acoustic causality i.e., points where new wave structure may be generated as a result of the nonlinear wave interaction [6]. In those cases it is required to apply an entropy correction to the scheme. This consists of determining the necessary viscosity to ensure correct formation of new waves ([8,9,13,21,25,29]).

In convex dynamics the points of acoustic causality are sonic points which are responsible for the formation of transonic rarefaction waves. Some numerical dissipation is required to guarantee correct formation of these waves avoiding the so-called "dog-leg" non-physical effect. In ideal MHD wave dynamics the points of acoustic causality are not only sonic points but the points where nonconvexity occurs too. Then, an additional entropy correction in the neighborhood of points where nonlinear characteristic fields are nonconvex is necessary to ensure correct formation of the peculiar complex wave structure of MHD equations as the so-called compound waves.

In this paper we study the nonconvex behavior of MHD equations through an analysis of the wave structure. From a scaled version of the Brio and Wu complete system of eigenvectors ([4,5]) and adopting the eight wave approach proposed by Powell et al. in [21] (see also [15]) we derive an analytical expression of the nonlinearity term associated to each nonlinear characteristic field. We obtain an explicit criterion to determine local regions of the solution for which a specific nonlinear wavefield becomes nonconvex. We then formulate an entropy-fix upwind scheme that uses the complete eigensystem of the MHD equations for the evaluation of the numerical fluxes and propose an entropy correction consisting of prescribing an analytical viscosity around points of acoustic causality (sonic and nonconvex points). The amount of viscosity is determined according to the analysis of the wave structure carried out and is applied locally in space and differently in each wavefield.

A third order version of the scheme is able to approximate the numerical solution of one and two-dimensional MHD Riemann problems, the evolution of the two-dimensional Orszag–Tang turbulence model ([7,19,20]) and the interaction between a strong shock and a high-density cloud ([8,2]). Numerical results indicate that the third order accurate entropy-fix upwind scheme behaves accurate, low dissipative and stable under high CFL numbers.

This paper is organized as follows. In Section 2 we analyze the wave structure of the ideal MHD equations and derive an analytical expression of the nonlinearity term for each characteristic field. In Section 3 we propose a nonconvex entropy-fix upwind scheme for scalar conservation laws and extend it for the equations of ideal MHD in Section 4. In Section 5 we explain the procedure to implement high order versions of our scheme and in Section 6 we present a set of numerical results. In Section 7 we draw our conclusions.

2. Ideal MHD equations: a nonconvex system of conservation laws

In this section we exhibit a scaled version of the complete system of eigenvectors proposed by Brio and Wu ([4,5]) adopting the eight wave approach presented by Powell et al. ([21]). The scaling guaranties continuity of the eigenvectors with respect to the conserved variables in the neighborhood of singular points. In addition, our unified way to express the nonlinear eigenvectors allows to derive an analytical expression of the nonlinearity term for the nonlinear characteristic fields. From this expression we discuss the nonconvexity of the ideal MHD equations for the two-dimensional case similarly as Brio and Wu stated in [4,5] for the one-dimensional case.

Let us consider a two-dimensional system of conservation laws of the form

$$\mathbf{u}_t + \mathbf{f}(\mathbf{u})_x + \mathbf{g}(\mathbf{u})_y = 0, \tag{5}$$

where $\mathbf{u} = (u_1, \ldots, u_m)$ is the vector of conserved variables and $\mathbf{f}(\mathbf{u}) = (f_1(\mathbf{u}), \ldots, f_m(\mathbf{u}))$ and $\mathbf{g}(\mathbf{u}) = (g_1(\mathbf{u}), \ldots, g_m(\mathbf{u}))$ are the fluxes. The system is hyperbolic if the Jacobians of the fluxes are diagonalizable matrices with real eigenvalues and a complete set of eigenvectors in each neighborhood of the solution ([17]). The diagonalization of the Jacobians decouples the original hyperbolic system in m scalar conservation laws defining the so-called characteristic fields and their corresponding characteristic fluxes ([16]).

Let $\lambda_1^f(\mathbf{u}), \ldots, \lambda_m^f(\mathbf{u})$ be the eigenvalues of the Jacobian $\mathbf{f}'(u)$ counting each one as many times as its multiplicity and $R^f = \{\mathbf{r}_1^f(\mathbf{u}), \ldots, \mathbf{r}_m^f(\mathbf{u})\}$ and $L^f = \{\mathbf{l}_1^f(\mathbf{u}), \ldots, \mathbf{l}_m^f(\mathbf{u})\}$ a complete system of right and left eigenvectors diagonalizing $f'(\mathbf{u})$ such that $\mathbf{r}_i^f \cdot \mathbf{l}_j^f = \delta_{ij}$ and

$$L^f(\mathbf{u})\mathbf{f}'(\mathbf{u})R^f(\mathbf{u}) = \Lambda = \operatorname{diag}(\lambda_1^f(\mathbf{u}), \ldots, \lambda_m^f(\mathbf{u})). \tag{6}$$

The eigenvalues of the Jacobian represent the characteristic speeds of the characteristic fluxes analogous to the first derivative of the flux of a scalar conservation law. The nonlinearity of the corresponding characteristic fields is determined by the scalar quantity $\nabla\lambda_k(\mathbf{u}) \cdot \mathbf{r}_k(\mathbf{u})$ that represents the second derivative of the scalar flux in a scalar conservation law [16].

A characteristic field "k" is said to be linearly degenerate if

$$\nabla\lambda_k(\mathbf{u}) \cdot \mathbf{r}_k(\mathbf{u}) \equiv 0 \tag{7}$$

and genuinely nonlinear or convex ([16]) if

$$\nabla\lambda_k(\mathbf{u}) \cdot \mathbf{r}_k(\mathbf{u}) \neq 0 \quad \forall \mathbf{u}. \tag{8}$$

Nonlinear characteristic fields that change acoustic phase in isolated points u_0 where $\nabla\lambda(\mathbf{u}_0) \cdot r(\mathbf{u}_0)$ vanishes are called non-convex ([12]).

Following the above formalism let us study the spectral structure of the ideal MHD equations.

The two-dimensional ideal MHD Eqs. (1)–(4) are a system of the form (5) where the conserved variables are $\mathbf{u} = (\rho, \rho\mathbf{v}, \mathbf{B}, E)^T$ being ρ the density, $\mathbf{v} = (u, v, w)$ the velocity field, $\mathbf{B} = (B_x, B_y, B_z)$ the magnetic field and E the total energy. The fluxes in each direction are defined as

$$f(\mathbf{u}) = \begin{bmatrix} \rho u \\ \rho u^2 + P^* - B_x^2 \\ \rho uv - B_xB_y \\ \rho uw - B_xB_z \\ 0 \\ uB_y - vB_x \\ uB_z - wB_x \\ u(E + P^*) - B_x(\mathbf{v} \cdot \mathbf{B}) \end{bmatrix}, \quad g(\mathbf{u}) = \begin{bmatrix} \rho v \\ \rho uv - B_xB_y \\ \rho v^2 + P^* - B_y^2 \\ \rho uw - B_zB_y \\ vB_x - uB_y \\ 0 \\ vB_z - wB_y \\ v(E + P^*) - B_y(\mathbf{v} \cdot \mathbf{B}) \end{bmatrix},$$

where $P^* = P + \frac{1}{2}\mathbf{B}^2$ is the total pressure and P the hydrodynamic pressure defined through the ideal gas EOS as $P = (\gamma - 1)\rho\epsilon$ with ϵ the specific internal energy.

In addition to this system of equations the magnetic field satisfies the divergence-free constraint

$$\nabla \cdot \mathbf{B} = 0. \tag{9}$$

To classify the characteristic fields of this MHD system we first present a spectral decomposition of the Jacobians such that the eigenvectors are smooth functions of the conserved variables. We show a complete system of eigenvectors of the Jacobian of $\mathbf{f}$ (x direction). The corresponding decomposition for the Jacobian of $\mathbf{g}$ (y direction) is similar.

We start from the normalization proposed in [5] carrying out the necessary modifications to satisfy the continuity condition.

Let us define $(b_x, b_y, b_z) = (B_x, B_y, B_z)/\sqrt{\rho}$ and $b^2 = b_x^2 + b_y^2 + b_z^2$. The acoustic sound speed is defined as

$$a = \sqrt{\frac{\gamma P}{\rho}}.$$

The Alfven velocity $c_a = |b_x|$ and the fast and slow velocities are given by

$$c_{f,s} = \sqrt{\frac{1}{2}\left[(a^2 + b^2) \pm \sqrt{(a^2 + b^2)^2 - 4a^2b_x^2}\right]}.$$

There are eight characteristic fields which characteristic velocities are: $\lambda_1(\mathbf{u}) = u - c_f, \lambda_2(\mathbf{u}) = u - c_a, \lambda_3(\mathbf{u}) = u - c_s, \lambda_4(\mathbf{u}) = u, \lambda_5(\mathbf{u}) = u, \lambda_6(\mathbf{u}) = u + c_s, \lambda_7(\mathbf{u}) = u + c_a, \lambda_8(\mathbf{u}) = u + c_f$.

We define $\mathrm{sgn}(t) = 1$ for $t \geqslant 0$ and $\mathrm{sgn}(t) = -1$ otherwise and set β_y and β_z values from the expressions

$$\beta_y = \begin{cases} \frac{B_y}{\sqrt{B_y^2+B_z^2}}; & B_y^2 + B_z^2 \neq 0, \\ \mathrm{sgn}(B_y)\frac{1}{\sqrt{2}}; & \text{otherwise}, \end{cases} \qquad \beta_z = \begin{cases} \frac{B_z}{\sqrt{B_y^2+B_z^2}}; & B_y^2 + B_z^2 \neq 0, \\ \mathrm{sgn}(B_z)\frac{1}{\sqrt{2}}; & \text{otherwise}. \end{cases}$$

The eigenvectors associated to $\lambda_4, \lambda_5, \lambda_2$ and λ_7, are

$$\begin{aligned}
\mathbf{r}_4 &= (1, u, v, w, 0, 0, 0, \frac{1}{2}q^2)^T, \\
\mathbf{r}_5 &= (0, 0, 0, 0, 1, 0, 0, B_x)^T, \\
\mathbf{l}_4 &= \frac{\gamma-1}{a^2}\left(1 - \frac{1}{2}q^2, u, v, w, B_x, B_y, B_z, -1\right), \\
\mathbf{l}_5 &= (0, 0, 0, 0, 1, 0, 0, 0)^T, \\
\mathbf{r}_2 &= \left(0, 0, -\beta_z \mathrm{sgn}(B_x), \beta_y \mathrm{sgn}(B_x), 0, -\frac{\beta_z}{\sqrt{\rho}}, \frac{\beta_y}{\sqrt{\rho}}, -\mathrm{sgn}(B_x)[\beta_z v - \beta_y w]\right)^T, \\
\mathbf{r}_7 &= \left(0, 0, -\beta_z \mathrm{sgn}(B_x), \beta_y \mathrm{sgn}(B_x), 0, \frac{\beta_z}{\sqrt{\rho}}, -\frac{\beta_y}{\sqrt{\rho}}, -\mathrm{sgn}(B_x)[\beta_z v - \beta_y w]\right)^T, \\
\mathbf{l}_2 &= \left(\frac{1}{2}\mathrm{sgn}(B_x)[\beta_z v - \beta_y w], 0, -\frac{\beta_z}{2}\mathrm{sgn}(B_x), \frac{\beta_y}{2}\mathrm{sgn}(B_x), 0, -\beta_z\frac{\sqrt{\rho}}{2}, \beta_y\frac{\sqrt{\rho}}{2}, 0\right), \\
\mathbf{l}_7 &= \left(\frac{1}{2}\mathrm{sgn}(B_x)[\beta_z v - \beta_y w], 0, -\frac{\beta_z}{2}\mathrm{sgn}(B_x), \frac{\beta_y}{2}\mathrm{sgn}(B_x), 0, \beta_z\frac{\sqrt{\rho}}{2}, -\beta_y\frac{\sqrt{\rho}}{2}, 0\right).
\end{aligned}$$

The eigenvectors associated to $\lambda_1, \lambda_3, \lambda_6$ and λ_8, can be expressed in an unified way for $k = 1, 3, 6, 8$ as

$$\begin{aligned}
\mathbf{r}_k = \Bigg(&\alpha, \alpha(u+c), \alpha v - \bar{\alpha}\bar{c}\,\mathrm{sgn}(c^2-a^2)\mathrm{sgn}(B_x)\beta_y, \alpha w - \bar{\alpha}\bar{c}, \mathrm{sgn}(c^2-a^2)\mathrm{sgn}(B_x)\beta_z, 0, \bar{\alpha}\frac{a}{\sqrt{\rho}}\mathrm{sgn}(c^2-a^2)\beta_y, \bar{\alpha}\frac{a}{\sqrt{\rho}}\mathrm{sgn}(c^2-a^2)\beta_z, \\
&\alpha\left(\frac{q^2}{2} + c^2 + uc - \frac{\gamma-2}{\gamma-1}a^2\right) - \mathrm{sgn}(c^2-a^2)\bar{\alpha}\bar{c}\,\mathrm{sgn}(B_x)(v\beta_y + w\beta_z)\Bigg),
\end{aligned} \tag{10}$$

$$\begin{aligned}
\mathbf{l}_k = \frac{1}{2a^2}\Bigg(&(\gamma-1)\alpha\frac{q^2}{2} - \alpha uc + \bar{\alpha}\bar{c}\,\mathrm{sgn}(c^2-a^2)\mathrm{sgn}(B_x)(v\beta_y + w\beta_z), (1-\gamma)\alpha u + \alpha c, \\
&(1-\gamma)\alpha v - \bar{\alpha}\bar{c}\,\mathrm{sgn}(c^2-a^2)\mathrm{sgn}(B_x)\beta_y, (1-\gamma)\alpha w - \bar{\alpha}\bar{c}\,\mathrm{sgn}(c^2-a^2)\mathrm{sgn}(B_x)\beta_z, -(1-\gamma)\alpha B_x, \\
&(1-\gamma)\alpha B_y + \sqrt{\rho}a\bar{\alpha}\,\mathrm{sgn}(c^2-a^2)\beta_y, (1-\gamma)\alpha B_z + \sqrt{\rho}a\bar{\alpha}\,\mathrm{sgn}(c^2-a^2)\beta_z, (\gamma-1)\alpha\Big),
\end{aligned} \tag{11}$$

where c and $\bar{c}$ and α and $\bar{\alpha}$ are determined as:

- for $k = 1$ and $k = 8, c = \mp c_f, \bar{c} = \mp c_s$ and

$$\alpha = \begin{cases} \alpha_f \cdot \mathrm{sgn}(B_y); & a^2 < b_x^2, \\ \alpha_f; & \text{otherwise}, \end{cases} \qquad \bar{\alpha} = \begin{cases} \alpha_s \cdot \mathrm{sgn}(B_y); & a^2 < b_x^2, \\ \alpha_s; & \text{otherwise}, \end{cases}$$

- for $k = 3$ and $k = 6, c = \mp c_s, \bar{c} = \mp c_f$ and

$$\alpha = \begin{cases} \alpha_s \cdot \mathrm{sgn}(B_y); & a^2 > b_x^2, \\ \alpha_s; & \text{otherwise}, \end{cases} \qquad \bar{\alpha} = \begin{cases} \alpha_f \cdot \mathrm{sgn}(B_y); & a^2 > b_x^2, \\ \alpha_f; & \text{otherwise}, \end{cases}$$

α_f and α_s are defined from the following expressions:

$$\alpha_f = \begin{cases} \sqrt{\frac{a^2-c_s^2}{c_f^2-c_s^2}}; & B_y^2 + B_z^2 \neq 0 \quad \text{or} \quad B_x^2 \neq \gamma P, \\ \frac{1}{\sqrt{2}}; & \text{otherwise}, \end{cases}$$

$$\alpha_s = \begin{cases} \sqrt{\frac{c_f^2-a^2}{c_f^2-c_s^2}}; & B_y^2 + B_z^2 \neq 0 \quad \text{or} \quad B_x^2 \neq \gamma P, \\ \frac{1}{\sqrt{2}}; & \text{otherwise}. \end{cases}$$

The system of eigenvectors for the Jacobian of $\mathbf{g}$ can be obtained by interchanging B_x by B_y, u by v, the second component by the third and the fifth by the sixth.

From the above spectral decomposition we shall study the wave structure of the MHD equations and analyze the convexity of the nonlinear fields in terms of the magnitude of the magnetic field.

The characteristic fields 2, 7 called Alfven waves, and 4, 5 called entropy waves or contacts are linearly degenerate since

$$\nabla\lambda_2(\mathbf{u})\cdot r_2(\mathbf{u})\equiv 0, \tag{12}$$
$$\nabla\lambda_7(\mathbf{u})\cdot r_7(\mathbf{u})\equiv 0, \tag{13}$$
$$\nabla\lambda_4(\mathbf{u})\cdot r_4(\mathbf{u})\equiv 0, \tag{14}$$
$$\nabla\lambda_5(\mathbf{u})\cdot r_5(\mathbf{u})\equiv 0. \tag{15}$$

The other fields are characterized and classified from the following statements.

Proposition 1. *If $\lambda(\mathbf{u})$ is an eigenvalue corresponding to a fast or slow characteristic field (1, 8 and 3, 6, respectively) and $\mathbf{r}(\mathbf{u})$ is the associated right eigenvector, then the following analytic expression is satisfied:*

$$\nabla\lambda(\mathbf{u})\cdot\mathbf{r}(\mathbf{u})=\frac{\alpha c}{2\rho}(1+2\bar{\alpha}^2+\gamma\alpha^2). \tag{16}$$

Proof. It follows from a nontrivial lengthy calculation from the proposed general expression of $\mathbf{r}(\mathbf{u})$ in terms of $\alpha,\bar{\alpha}$ and c. □

Corollary 1. *Expression (16) does not vanish identically for fast and slow characteristic fields. Therefore, these characteristic fields are nonlinear.*

The following theorem describes the conditions under which a nonlinear characteristic field (fast or slow) is nonconvex in terms of the change of sign of the components of the magnetic field.

Theorem 1. *Let us assume $B_z=0$*

(1) *If $a^2<b_x^2$, then:*
   (a) *The slow wavefields are genuinely nonlinear*
   (b) *The fast wavefields are non-genuinely nonlinear (nonconvex) and for each fast eigenvalue $\lambda(\mathbf{u})$ and its associated eigenvector $r(u)$, the scalar quantity $\nabla\lambda(\mathbf{u})\cdot\mathbf{r}(\mathbf{u})$ vanishes if and only if $B_y=0$, and changes sign with B_y.*

(2) *If $a^2>b_x^2$, then:*
   (a) *The fast wavefields are genuinely nonlinear.*
   (b) *The slow wavefields are non-genuinely nonlinear (nonconvex) and for each slow eigenvalue $\lambda(\mathbf{u})$ and its associated eigenvector $\mathbf{r}(\mathbf{u})$ the scalar quantity $\nabla\lambda(\mathbf{u})\cdot\mathbf{r}(\mathbf{u})$ vanishes if and only if either $B_y=0$ or $B_x=0$, and $\nabla\lambda(\mathbf{u})\cdot\mathbf{r}(\mathbf{u})$ changes sign with B_y.*

Proof. (1-a) If $\lambda(\mathbf{u})$ is a slow eigenvalue and $\mathbf{r}(\mathbf{u})$ its associated eigenvector then the expression (16) becomes

$$\nabla\lambda(\mathbf{u})\cdot\mathbf{r}(\mathbf{u})=\pm\frac{\alpha_s c_s}{2\rho}\left(1+2\bar{\alpha}_f^2+\gamma\alpha_s^2\right) \tag{17}$$

because $\alpha=\alpha_s,\bar{\alpha}=\alpha_f$ and $c=\pm c_s$ in this case.

From $a^2\leqslant b_x^2\leqslant c_f^2$ it follows that $\alpha_s>0$ and $c_s>0$ since $a^2b_x^2>0$. Thus $\nabla\lambda(\mathbf{u})\cdot\mathbf{r}(\mathbf{u})\neq 0$ for all $\mathbf{u}$.

(1-b) If $\lambda(\mathbf{u})$ is a fast eigenvalue then $\alpha=\ \mathrm{sgn}(B_y)\alpha_f$ and $c=\pm c_f$. Since $\alpha_f^2\alpha_s^2=\frac{a^2b_y^2}{c_f^2-c_s^2}$ and $c_s^2\leqslant a^2<b_x^2\leqslant c_f^2$ we have that

$$\alpha_f^2=\frac{a^2b_y^2}{c_f^2-a^2}. \tag{18}$$

Thus, from expression (16) in Proposition 1, $\nabla\lambda(\mathbf{u})\cdot\mathbf{r}(\mathbf{u})=0$ if and only if $B_y=0$.

(2-a) If $\lambda(\mathbf{u})$ is a fast eigenvalue and $\mathbf{r}(\mathbf{u})$ its associated eigenvector then (16) becomes

$$\nabla\lambda(\mathbf{u})\cdot\mathbf{r}(\mathbf{u})=\pm\frac{\alpha_f c_f}{2\rho}\left(1+2\bar{\alpha}_s^2+\gamma\alpha_f^2\right) \tag{19}$$

because $\alpha=\alpha_f,\bar{\alpha}=\alpha_s$ and $c=\pm c_f$ in this case.

From $a^2>b_x^2\geqslant c_s^2$ we have that $\alpha_f>0$. On the other hand c_f is always different from zero and $1+2\alpha_s^2+\gamma\alpha_f^2\geqslant 1$. Therefore $\nabla\lambda(\mathbf{u})\cdot\mathbf{r}(\mathbf{u})\neq 0$ for all u.

(2-b) If $\lambda(\mathbf{u})$ is a slow eigenvalue then $\alpha=\ \mathrm{sgn}(B_y)\alpha_s$ and $c=\pm c_s$. Since $c_s^2\leqslant b_x^2<a^2\leqslant c_f^2$ we have that

$$\alpha_s^2=\frac{a^2b_y^2}{a^2-c_s^2}. \tag{20}$$

Thus, from expression (16) in Proposition 1, $\nabla\lambda(\mathbf{u})\cdot\mathbf{r}(\mathbf{u})=0$ if and only if either $B_y=0$ or $c_s=0$. Since $c_f>0$ and $c_sc_f=a^2b_x^2$ then $c_s=0$ if and only if $B_x=0$.

Remark 1. Theorem 1 follows for y-direction interchanging B_y by B_x.

Remark 2. When B_y changes sign either the fast or the slow characteristic fields in the x-direction are nonconvex and consequently the slow characteristic fields in the y-direction become nonconvex. The same apply in the y-direction when B_x changes sign.

Remark 3. The analysis concludes that the characteristic velocities of the fast fields (for $a^2 < b_x^2$) and the slow fields (for $a^2 > b_x^2$) are non-monotone functions of B_y.

Remark 4. Proposition 1 extends to the two-dimensional case the discussion of nonconvexity performed by Brio and Wu in [4,5]. The calculation of $\nabla\lambda(\mathbf{u})$ in general expression (16) accounts for possible vanishing of the nonlinearity term when $B_x = 0$ (in the x-direction). In particular, the case considered in expression (17) shows that the slow nonlinear characteristic field in the x-direction might become nonconvex not only when B_y (transversal magnetic field) vanishes but when B_x does.

The analytical study carried out supplies a criterion to characterize local regions containing points of acoustic causality inherent to the MHD equations. The description allows us to perform a specific numerical treatment for the nonconvex characteristic fields as we will develop in the following.

3. An entropy-fix upwind scheme for nonconvex scalar conservation laws

A numerical scheme based on the local characteristic decomposition of a system of conservation laws considers each of the characteristic fields as a scalar conservation law. As we have seen in the previous section, the decoupled system of MHD equations counts with several nonlinear characteristic fields that might be nonconvex. In this section we propose an upwind numerical scheme for the approximation of the solution of nonconvex scalar conservation laws.

The one-dimensional case of a scalar conservation law can be written as

$$u_t + f(u)_x = 0 \quad \text{with } u(x,0) = u_0(x), \tag{21}$$

where $u_0(x)$ is piecewise smooth, periodic or of compact support. The conservation law (21) is governed by the flux $f(u)$ that is a twice differentiable nonlinear function. A conservation law is convex if $f''(u) \neq 0\ \forall u$ and is nonconvex if $f''(u)$ vanishes in some isolated points: points where phase change occurs ([12,13]).

A scheme in conservation form for a scalar conservation law is written as

$$u_j^{n+1} = u_j^n - \frac{\Delta t}{\Delta x}\left(\tilde{f}_{j+\frac{1}{2}} - \tilde{f}_{j-\frac{1}{2}}\right), \tag{22}$$

where $u_j^n \approx u(x_j, t_n)$ is a numerical approximation of the weak solution of (21) defined in the computational cell $x_j = jh, t_n = n\Delta t$. The numerical flux $\tilde{f}_{j+\frac{1}{2}}^n$ is a function of $2k$ variables $\tilde{f}_{j+\frac{1}{2}} = \tilde{f}(u_{j-k+1}, \ldots, u_{j+k})$ that is consistent with (21), i.e. $\tilde{f}(u, \ldots, u) = f(u)$.

An upwind scheme in conservation form for a nonlinear scalar conservation law computes the numerical fluxes according to the sign of the local wave speed $f'(u)$. The main advantage of these schemes lies on the low dissipation of the approximation of the solution. This behavior allows to capture fine structure of the solution better than other dissipative schemes. On the contrary, upwind schemes fail to be monotone in the neighborhood of points where new structure is generated [25]. Transonic rarefactions around sonic points (where $f'(u)$ changes sign) and compound waves around phase points (where $f''(u)$ changes sign) are not well resolved by the upwind strategy. In fact, these points of acoustic causality need of numerical dissipation to be able to develop their intrinsic structures.

In [25], Shu and Osher proposed the so-called "entropy-fix upwind scheme" as an entropy correction to upwind schemes for convex fluxes prescribing the necessary viscosity to avoid "dog-leg" effect in transonic rarefactions. The correction consists in switching to a Lax–Friedrichs scheme around sonic points. We refer to this scheme as sonic-fix upwind (SFU) scheme. The numerical flux $\tilde{f}_{j+\frac{1}{2}}^n := g_{SFU}(u_j^n, u_{j+1}^n)$ is defined as

$$g_{SFU}(u_j^n, u_{j+1}^n) = \begin{cases} g_{LF}(u_j^n, u_{j+1}^n) & \text{if } f'(u_j^n)\cdot f'(u_{j+1}^n) < 0 \text{ (sonic points)} \\ g_{UPW}(u_j^n, u_{j+1}^n) & \text{otherwise} \end{cases}$$

being g_{LF} the Lax–Friedrichs flux

$$g_{LF}(u,v) = \frac{1}{2}(f(u) + f(v)) - \frac{\alpha}{2}(v-u), \tag{23}$$

where the analytical viscosity is defined as $\alpha := \max_{w\in[u,v]}|f'(w)|$ and the upwind flux defined as ([22,25])

$$g_{UPW}(u,v) = \begin{cases} f(u) & \text{if } f\left(\frac{u+v}{2}\right) \geqslant 0 \\ f(v) & \text{if } f\left(\frac{u+v}{2}\right) < 0 \end{cases}$$

Next we propose to extend the entropy correction to nonconvex dynamics with a similar procedure to allow correct formation of compound waves in the neighborhood of phase points.

Our entropy-fix upwind (EFU) scheme for a nonconvex scalar conservation law defines the numerical flux as

$$g_{EFU}(u_j^n, u_{j+1}^n) = \begin{cases} g_{LF}(u_j^n, u_{j+1}^n), & \text{if} \begin{cases} f'(u_j^n)\cdot f'(u_{j+1}^n) < 0 \quad \text{(sonic points)}, \\ \text{or} \\ f''(u_j^n)\cdot f''(u_{j+1}^n) < 0 \quad \text{(phase points)} \end{cases} \\ g_{UPW}(u_j^n, u_{j+1}^n), & \text{otherwise} \end{cases}$$

As an illustration of the significance of performing an entropy correction on points of acoustic causality as sonic points and phase points for the approximation of the solution of convex and nonconvex scalar conservation laws we perform the numerical approximation of two initial-value problems associated to the convex Burgers and nonconvex Buckley–Leverett fluxes.

We consider the scalar conservation law (21) with f_1 and f_2, convex and nonconvex fluxes, respectively

$$f_1(u) = \frac{u^2}{2}; \quad f_2(u) = \frac{4u^2}{4u^2 + (1-u)^2} \tag{24}$$

and the corresponding u_1 and u_2 initial data in $[-1,1]$

$$u_1(x) = \begin{cases} -\frac{1}{2}, & x \leqslant 0, \\ 1, & \text{otherwise}, \end{cases} \qquad u_2(x) = \begin{cases} 1, & 0 \leqslant x \leqslant 0.5, \\ 0, & \text{otherwise}. \end{cases}$$

The flux function $f_1(u)$ contains a sonic point at $u = 0$ and is convex since $f''(u) > 0\ \forall u \in [-1,1]$. Flux function $f_2(u)$ is nonconvex since contains a state $u_1 \approx 0.2871$ such that $f''(u_1) = 0$ and $f''(u) \neq 0\ \forall u \in [-1,1], u \neq u_1$. We compute first order accurate numerical approximations of the solution of both problems using 200 points at time $t = 0.4$ and a Courant–Friedrichs–Lewy (CFL) coefficient equal to 0.8.

In the convex case we compare UPW, SFU schemes and the more dissipative standard Lax–Friedrichs scheme versus the exact solution of the problem. In the nonconvex case we compare both entropy-fix upwind schemes for convex and nonconvex fluxes, SFU and EFU respectively, and the Lax–Friedrichs scheme versus the exact solution of the problem.

Fig. 1 left displays convergence to the correct solution by Lax–Friedrichs scheme. Central picture in the same figure shows how upwind scheme fails to converge to the entropy solution. Right picture of Fig. 1 displays the result with the Shu–Osher sonic-fix upwind (SFU) scheme. The viscosity prescription at the sonic point allows convergence to the entropy solution.

In Fig. 2 left we observe convergence to the entropy solution by Lax–Friedrichs method although the approximation is poor due to the excessive dissipation of the scheme. The convex sonic-fix upwind scheme (Fig. 2, center) does not converge to the entropy solution because selects the upwind choice at phase points. Right picture of Fig. 2 displays the result with our entropy-fix upwind scheme showing convergence to the exact solution with reduced dissipation. The good resolution obtained with our scheme demonstrates the advantage of upwind schemes to approximate the correct entropy solution when combined with an appropriate prescription of the viscosity at points of acoustic causality.

In the following section we extend the proposed scheme to the MHD system of conservation laws where nonlinear characteristic fields might be nonconvex.

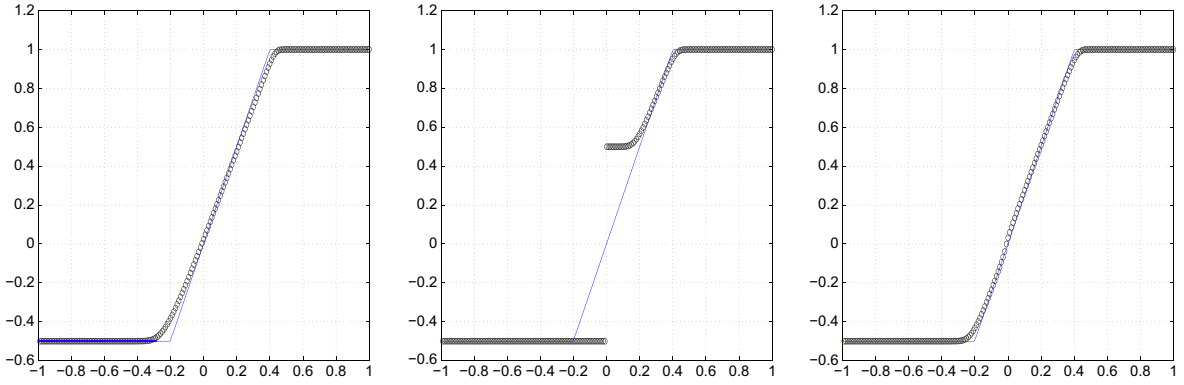

Fig. 1. Exact solution (solid line) versus approximate solutions at time $t = 0.4$ with 200 grid points and $CFL = 0.8$ of the Burgers problem for the Lax–Friedrichs scheme (left), upwind scheme (center) and sonic-fix upwind scheme (right).

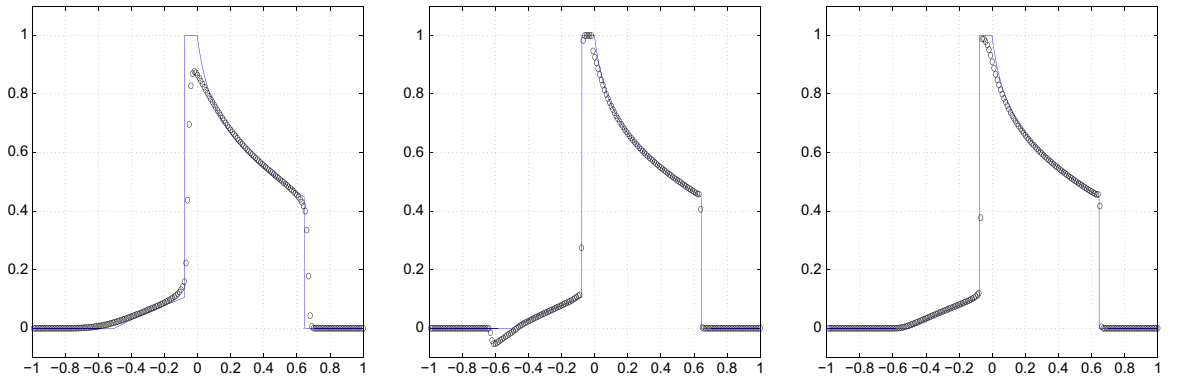

Fig. 2. Exact solution (solid line) versus approximate solutions at time $t = 0.4$ with 200 grid points and $CFL = 0.8$ of the Buckley–Leverett problem for the Lax–Friedrichs scheme (left), sonic-fix upwind scheme (center) and nonconvex entropy-fix upwind scheme (right).

4. An entropy-fix upwind scheme for the equations of ideal magnetohydrodynamics

The diagonalization of the Jacobians of the fluxes decouples the original system of conservation laws into a system of scalar conservation laws local in space and time. In this section we adopt the local characteristic decomposition approach presented in Section 2 and design a characteristic-based upwind scheme for the ideal MHD equations. We propose an entropy correction around points of acoustic causality in accordance with the analytical study carried out in Section 2 to characterize nonconvex points. We prescribe a specific local viscosity in a similar way as proposed in Section 3 for nonconvex scalar conservation laws.

A numerical scheme in conservation form for a system of conservation laws in two dimensions can be written as

$$\mathbf{u}_{jk}^{n+1} = \mathbf{u}_{jk}^{n} - \frac{\Delta t}{\Delta x}\left(\tilde{\mathbf{f}}_{j+\frac{1}{2},k} - \tilde{\mathbf{f}}_{j-\frac{1}{2},k}\right) - \frac{\Delta t}{\Delta y}\left(\tilde{\mathbf{g}}_{j,k+\frac{1}{2}} - \tilde{\mathbf{g}}_{j,k-\frac{1}{2}}\right), \tag{25}$$

where $\tilde{\mathbf{f}}$ and $\tilde{\mathbf{g}}$ are the numerical fluxes in each direction consistent with the fluxes of the system.

We perform in each direction the local characteristic decomposition of this system decoupling the equations in linearly independent characteristic fields. We design our numerical scheme applying to each characteristic field a similar procedure as the one proposed in Section 3 for scalar conservation laws. We select the upwind choice for the computation of numerical fluxes at upwind interfaces and we correct entropy in all characteristic fields at interfaces containing points of acoustic causality: sonic points and nonconvex points (singular points where the transverse magnetic field changes sign).

The entropy correction proposed for singular points consists of applying the Lax–Friedrichs flux splitting procedure to each characteristic field prescribing a viscosity α that in the x-direction reads as

$$\alpha^x = \max\left(\left|\lambda_4^f(\mathbf{u}_{jk}^n)\right|, \left|\lambda_4^f(\mathbf{u}_{j+1,k}^n)\right|\right) + \max\left(c_{jk}^x, c_{j+1,k}^x\right), \tag{26}$$

where $c_{jk}^x = \sqrt{c_f^x\left(\mathbf{u}_{jk}^n\right)^2 + c_s^x(\mathbf{u}_{jk}^n)^2}$ and $c_{j+1,k}^x = \sqrt{c_f^x(\mathbf{u}_{j+1,k}^n)^2 + c_s^x(\mathbf{u}_{j+1,k}^n)^2}$.

This α^x value is an upper bound of the maximum of the absolute values of the allowed characteristic speeds since $c_f^x \leqslant \sqrt{c_f^{x2} + c_s^{x2}} = \sqrt{a^2 + b^2}$. We choose λ_4 because the characteristic field $p = 4$ corresponds to the entropy contact wave and therefore $\lambda_4^f(\mathbf{u})$ is the x-component of the fluid velocity. For the y-direction case the viscosity α^y is defined in terms of c_{jk}^y and $c_{j,k+1}^y$ and the y-component of the fluid velocity $\lambda_5^g(\mathbf{u})$. This entropy correction provides a suitable amount of viscosity allowing the correct formation of compound waves.

The entropy correction at sonic points consists in prescribing the viscosity as the maximum of absolute values of the local wave speeds at both sides of the interfaces ([25]).

Next we propose an specific first order accurate numerical scheme to approximate the solution of the ideal MHD equations.

Numerical schemes for hyperbolic conservation laws based on characteristic field decomposition are required to satisfy the Rankine–Hugoniot relations to approximate the numerical fluxes of the scheme ([16,17]). Those numerical schemes that use one linearization at interfaces need of explicit formulas to compute an average state at interfaces ([22]). There exist exact formulas for the ideal MHD system only for the case where the adiabatic exponent γ is $\gamma = 2$ ([5]). For other values of γ there are not such formulas to satisfy exactly Rankine–Hugoniot relations and arithmetic averages are used instead to define the intermediate states ([5,15]). The arbitrary averaging satisfies approximately Rankine–Hugoniot relations although it might define non-physical intermediate states.

We are interested in solving MHD problems for different values of γ preventing from computing averages at interfaces. We then will approximate the numerical fluxes at cell interfaces by means of two linearizations at each side of the interface following the interface splitting strategy used in the Marquina flux formula (MFF) [9] that satisfies approximately Rankine–Hugoniot relations avoiding any averaging at interfaces.

The specific form of the first order accurate approximation of the system of equations reads as

$$\mathbf{u}_{jk}^{n+1} = \mathbf{u}_{jk}^{n} - \frac{\Delta t}{\Delta x}\left(\tilde{\mathbf{f}}(\mathbf{u}_{jk}^{n}, \mathbf{u}_{j+1,k}^{n}) - \tilde{\mathbf{f}}(\mathbf{u}_{j-1,k}^{n}, \mathbf{u}_{jk}^{n})\right) - \frac{\Delta t}{\Delta y}\left(\tilde{\mathbf{g}}(\mathbf{u}_{jk}^{n}, \mathbf{u}_{j,k+1}^{n}) - \tilde{\mathbf{g}}(\mathbf{u}_{j,k-1}^{n}, \mathbf{u}_{jk}^{n})\right) \tag{27}$$

such that $\tilde{\mathbf{f}}(\mathbf{u},\mathbf{u}) = \mathbf{f}(\mathbf{u})$ and $\tilde{\mathbf{g}}(\mathbf{u},\mathbf{u}) = \mathbf{g}(\mathbf{u})$.

The first order accurate flux splitting formula to compute $\tilde{\mathbf{f}}$ (similar for $\tilde{\mathbf{g}}$) in terms of two linearizations for each flux and interface as proposed in [9] is

$$\tilde{\mathbf{f}}(\mathbf{u}_{jk}^{n}, \mathbf{u}_{j+1,k}^{n}) = \sum_{p=1}^{8}\left[\psi_{+}^{p}\mathbf{r}_{p}^{f}\left(\mathbf{u}_{jk}^{n}\right) + \psi_{-}^{p}\mathbf{r}_{p}^{f}(\mathbf{u}_{j+1,k}^{n})\right], \tag{28}$$

where the lateral numerical characteristic fluxes ψ_{+}^{p} and ψ_{-}^{p} at the interfaces are determined as detailed in the following.

We compute the complete system of eigenvectors at $\mathbf{u}_{jk}^{n}$ and $\mathbf{u}_{j+1,k}^{n}$ and the associated eigenvalues $\lambda_{p}^{f}(\mathbf{u}_{jk}^{n})$ and $\lambda_{p}^{f}(\mathbf{u}_{j+1,k}^{n})$ for $p = 1, 2, \ldots, 8$ proposed in Section 2. The local characteristic fluxes and variables are calculated at both sides of the interface as

$$\phi_{j,k}^{p} = \mathbf{f}(\mathbf{u}_{jk}^{n}) \cdot \mathbf{l}_{p}^{f}(\mathbf{u}_{jk}^{n}), \tag{29}$$

$$\phi_{j+1,k}^{p} = \mathbf{f}(\mathbf{u}_{j+1,k}^{n}) \cdot \mathbf{l}_{p}^{f}(\mathbf{u}_{j+1,k}^{n}), \tag{30}$$

$$w_{j,k}^{p} = \mathbf{u}_{j,k}^{n} \cdot \mathbf{l}_{p}^{f}(\mathbf{u}_{jk}^{n}), \tag{31}$$

$$w_{j+1,k}^{p} = \mathbf{u}_{j+1,k}^{n} \cdot \mathbf{l}_{p}^{f}(\mathbf{u}_{j+1,k}^{n}) \tag{32}$$

for $p = 1, 2, \ldots, 8$.

Then the numerical characteristic fluxes ψ_{+}^{p} and ψ_{-}^{p} are determined from the following procedure and are expressed in terms of $\phi_{j+\frac{1}{2},k}^{+p}, \phi_{j+\frac{1}{2},k}^{-p}, w_{j+\frac{1}{2},k}^{+p}$ and $w_{j+\frac{1}{2},k}^{-p}$ which represent the extended values at the interface of the characteristic fluxes and variables. First order approximation of these values through extensions by constant are $\phi_{jk}^{p}, \phi_{j+1,k}^{p}, w_{jk}^{p}$ and $w_{j+1,k}^{p}$, respectively.

- If $\left(x_{j+\frac{1}{2}}, y_{k}\right)$ is a *singular interface* ($\left(B_{y}(x_{j}, y_{k}) \cdot B_{y}(x_{j+1}, y_{k}) \leqslant 0 \text{ and } a^{2} < b_{x}^{2} \text{ or } a^{2} > b_{x}^{2}\right)$ or $(B_{x}(x_{j}, y_{k}) \cdot B_{x}(x_{j+1}, y_{k}) \leqslant 0$ and $a^{2} > b_{x}^{2}$), i.e., the interface contains a nonconvex point under Theorem 1 conditions) then,

  $$\alpha^{x} = \max\left(\left|\lambda_{4}^{f}\left(\mathbf{u}_{jk}^{n}\right)\right|, \left|\lambda_{4}^{f}\left(\mathbf{u}_{j+1,k}^{n}\right)\right|\right) + \max\left(c_{jk}^{x}, c_{j+1,k}^{x}\right),$$

  where

  $$c_{jk}^{x} = \sqrt{c_{f}^{x}(\mathbf{u}_{jk}^{n})^{2} + c_{s}^{x}(\mathbf{u}_{jk}^{n})^{2}} \quad \text{and} \quad c_{j+1,k}^{x} = \sqrt{c_{f}^{x}(\mathbf{u}_{j+1,k}^{n})^{2} + c_{s}^{x}(\mathbf{u}_{j+1,k}^{n})^{2}}$$

  and the numerical fluxes are defined as:

  $$\psi_{+}^{p} = \frac{1}{2}\left(\phi_{j+\frac{1}{2},k}^{+p} + \alpha w_{j+\frac{1}{2},k}^{+p}\right); \quad \psi_{-}^{p} = \frac{1}{2}\left(\phi_{j+\frac{1}{2},k}^{-p} - \alpha w_{j+\frac{1}{2},k}^{-p}\right) \tag{33}$$

  for $p = 1, 2, \ldots, 8$.
- If $\left(x_{j+\frac{1}{2}}, y_{k}\right)$ is a *sonic interface* (there is at least one $q \in \{1, 2, \ldots, 8\}$ such that $\lambda_{q}^{f}(\mathbf{u}_{j,k}^{n}) \cdot \lambda_{q}^{f}(\mathbf{u}_{j+1,k}^{n}) \leqslant 0$) then

  $$\alpha_{p} = \max\left(\left|\lambda_{p}^{f}\left(\mathbf{u}_{jk}^{n}\right)\right|, \left|\lambda_{p}^{f}\left(\mathbf{u}_{j+1,k}^{n}\right)\right|\right) \tag{34}$$

  and the numerical fluxes are defined as

  $$\psi_{+}^{p} = \frac{1}{2}\left(\phi_{j+\frac{1}{2},k}^{+p} + \alpha_{p} w_{j+\frac{1}{2},k}^{+p}\right); \quad \psi_{-}^{p} = \frac{1}{2}\left(\phi_{j+\frac{1}{2},k}^{-p} - \alpha_{p} w_{j+\frac{1}{2},k}^{-p}\right) \tag{35}$$

  for $p = 1, 2, \ldots, 8$.
- If $\left(x_{j+\frac{1}{2}}, y_{k}\right)$ is an *upwind interface* (an interface not containing points of acoustic causality) then
  - If $\lambda_{p}^{f}\left(u_{jk}^{n}\right) > 0$,

    $$\psi_{+}^{p} = \phi_{j+\frac{1}{2},k}^{+p}; \quad \psi_{-}^{p} = 0. \tag{36}$$

  - If $\lambda_{p}^{f}\left(u_{jk}^{n}\right) \leqslant 0$,

    $$\psi_{+}^{p} = 0; \quad \psi_{-}^{p} = \phi_{j+\frac{1}{2},k}^{-p} \tag{37}$$

    for $p = 1, 2, \ldots, 8$.

The calculation of $\tilde{\mathbf{g}}$ at interface $\left(x_j, y_{k+\frac{1}{2}}\right)$ is similar taking into account the corresponding condition of Theorem 1 for the y-direction case, (Remark 1 in Section 2).

Last step to approximate the solution of the two-dimensional MHD system of equations consists of enforcing (9), the divergence-free constraint on the magnetic field.

The re-projection step involves the global solution of an elliptic equation with a non-smooth source term ([3,26]). This induces extra dissipation on the magnetic field since the general solution of this equation can be expressed as a global convolution operator with a smooth kernel. The extra dissipation added on the magnetic field induces dissipation to the rest of conserved quantities since these variables are strongly coupled. Therefore, the re-projection step implies a global dissipation over a set of conserved variables that are (in fact) approximated locally in space through a hyperbolic system of equations.

It is essential for most numerical schemes to perform the mentioned additional correction on the magnetic field to satisfy the divergence-free constraint ensuring stability and accuracy of the scheme [8,10,15,26]. We remark that some numerical schemes proposed recently do not need to enforce this constraint [1,2].

In our calculations the correction of the magnetic field to satisfy the divergence-free constraint is applied at the end of every time step following the prescription proposed in [3].

We first compute, by a fast Poisson solver, the approximate solution ϕ of

$$\Delta\phi + \nabla\cdot\mathbf{B} = 0 \tag{38}$$

being $\mathbf{B}$ the magnetic field to be corrected, and we set the corrected magnetic field $\mathbf{B}^c$ computed as

$$\mathbf{B}^c = \mathbf{B} + \nabla\phi. \tag{39}$$

We use central differences for the computation of $\nabla\cdot\mathbf{B}, \nabla\phi$ and $\Delta\phi$ ensuring that $\nabla\cdot\mathbf{B} = 0$ is preserved up to the truncation error of the method.

The proposed upwind scheme for ideal MHD equations presented in this section corrects entropy in the neighborhood of points where new wave structure is generated as an alternative to the upwind strategy. The entropy correction is performed in each characteristic wavefield according to an appropriate viscosity that is consistent with the nonconvex behavior of the MHD equations and is made locally in space and time over all characteristic fields around sonic and singular points. The proposed numerical scheme is well behaved since the numerical fluxes are computed through a flux formula that is a continuous function of the conserved variables ([13]).

5. High order numerical implementation

In this section we explain the procedure we follow to obtain high order accurate approximations of the solution of the ideal MHD system of equations.

We consider the first order entropy-fix upwind scheme proposed in the previous section to approximate the numerical fluxes of the scheme in conservation form (27) and we apply a reconstruction procedure on local characteristic fluxes and variables following the so-called "flux formulation" ([25]) to achieve high order accuracy in space. We perform this procedure dimension-by-dimension to obtain a two-dimensional conservative approximation. We then apply a high order total variation diminishing (TVD) Runge–Kutta time stepping procedure for the integration in time ([25]). The algorithm to achieve high order accuracy in space is as follows.

Let us consider a reconstruction function R which has a $2l+1$ points stencil and let $\hat{z}$ represent the high order spatial approximation of z. The first order Euler explicit approximation in time and high order accurate spatial approximation of the conserved variables of our system based in the expression (27) becomes

$$\mathbf{u}_{jk}^{n+1} = \mathbf{u}_{jk}^{n} - \frac{\Delta t}{\Delta x}\left(\hat{\tilde{\mathbf{f}}}_{j+\frac{1}{2},k}^{n} - \hat{\tilde{\mathbf{f}}}_{j-\frac{1}{2},k}^{n}\right) - \frac{\Delta t}{\Delta y}\left(\hat{\tilde{\mathbf{g}}}_{j,k+\frac{1}{2}}^{n} - \hat{\tilde{\mathbf{g}}}_{j,k-\frac{1}{2}}^{n}\right), \tag{40}$$

where the numerical fluxes $\hat{\tilde{f}}$ and $\hat{\tilde{g}}$ at each interface $x_{j+\frac{1}{2}}$ and $x_{j-\frac{1}{2}}$ in the x- and y-directions respectively are functions of $2l+2$ conserved variables.

We compute these numerical fluxes using two linearizations at each interface following Marquina's interface splitting procedure [9]. The resulting flux splitting for $\hat{\tilde{f}}$ at the right interface $x_{j+\frac{1}{2},k}$ is computed from the characteristic numerical fluxes at both sides of the interface as

$$\hat{\tilde{\mathbf{f}}}_{j+\frac{1}{2},k}^{n} = \sum_{p=1}^{8}\left[\hat{\psi}_{+}^{p}(\mathbf{u}_{j-l,k},\ldots,\mathbf{u}_{j+l,k})\mathbf{r}_{p}^{f}\left(\mathbf{u}_{jk}^{n}\right) + \tilde{\psi}_{-}^{p}(\mathbf{u}_{j-l+1,k},\ldots,\mathbf{u}_{j+l+1,k})\mathbf{r}_{p}^{f}(\mathbf{u}_{j+1,k}^{n})\right], \tag{41}$$

where $\hat{\psi}_{+}^{p}$ and $\hat{\psi}_{-}^{p}$ are the high order accurate characteristic numerical fluxes computed through formulas (33), (35), (36) or (37) in terms of the high order accurate values of the characteristic fluxes and variables $\hat{\phi}_{j+\frac{1}{2},k}^{+p}$, $\hat{\phi}_{j+\frac{1}{2},k}^{-p}$, $\hat{w}_{j+\frac{1}{2},k}^{+p}$ and $\hat{w}_{j+\frac{1}{2},k}^{-p}$ at both sides of the interface. These are calculated from $2l+1$ first order characteristic fluxes and variables respectively by evaluating at the interface a reconstruction function R that is determined via primitive function and satisfies the conservation property ([25]). The function R must be an elementary function that approximates the corresponding variable or flux up to a degree of accuracy.

Thus, $\hat{\phi}^{+p}_{j+\frac{1}{2},k} = R_{\phi^+}\left(x_{j+\frac{1}{2}}\right)$ such that R_{ϕ^+} satisfies

$$\phi^{+p}_{j,k} = \frac{1}{h}\int_{x_{j-\frac{1}{2}}}^{x_{j+\frac{1}{2}}} R_{\phi^+}\left(\phi^{+p}_{j-l,k},\ldots,\phi^{+p}_{j+l,k};s\right)ds,$$

where $\phi^{+p}_{i,k} = \mathbf{f}\left(\mathbf{u}^n_{i,k}\right)\cdot\mathbf{l}^f_p\left(\mathbf{u}^n_{jk}\right),\ i = j-l,\ldots,j+l.$

Similarly,

- $\hat{w}^{+p}_{j+\frac{1}{2},k} = R_{w^+}\left(x_{j+\frac{1}{2}}\right)$ in terms of $w^{+p}_{i,k} = \mathbf{u}^n_{i,k}\cdot\mathbf{l}^f_p\left(\mathbf{u}^n_{jk}\right), i = j-l,\ldots,j+l$, such that
$$w^{+p}_{j,k} = \frac{1}{h}\int_{x_{j-\frac{1}{2}}}^{x_{j+\frac{1}{2}}} R_{w^+}\left(w^{+p}_{j-l,k},\ldots,w^{+p}_{j+l,k};s\right)ds.$$
- $\hat{\phi}^{-p}_{j+\frac{1}{2},k} = R_{\phi^-}\left(x_{j+\frac{1}{2}}\right)$ in terms of $\phi^{-p}_{i,k} = \mathbf{f}\left(\mathbf{u}^n_{i,k}\right)\cdot\mathbf{l}^f_p\left(\mathbf{u}^n_{j+1,k}\right),\ i = j-l+1,\ldots,j+l+1$, such that
$$\phi^{-p}_{j+1,k} = \frac{1}{h}\int_{x_{j+\frac{1}{2}}}^{x_{j+\frac{3}{2}}} R_{\phi^-}\left(\phi^{-p}_{j-l+1,k},\ldots,\phi^{-p}_{j+l+1,k};s\right)ds.$$
- $\hat{w}^{-p}_{j+\frac{1}{2},k} = R_{w^-}\left(x_{j+\frac{1}{2}}\right)$ in terms of $w^{-p}_{i,k} = \mathbf{u}^n_{i,k}\cdot\mathbf{l}^f_p\left(\mathbf{u}^n_{j+1,k}\right), i = j-l+1,\ldots,j+l+1$, such that
$$w^{-p}_{j+1,k} = \frac{1}{h}\int_{x_{j+\frac{1}{2}}}^{x_{j+\frac{3}{2}}} R_{w^-}\left(w^{-p}_{j-l+1,k},\ldots,w^{-p}_{j+l+1,k};s\right)ds.$$

The flux splitting for $\hat{\hat{f}}$ at the left interface $x_{j-\frac{1}{2},k}$ is computed similarly to (41) shifting the index j one unit to the left, $\hat{\hat{\mathbf{f}}}^n_{j-\frac{1}{2},k} = \hat{\hat{\mathbf{f}}}^n_{j-\frac{1}{2},k}(\mathbf{u}^n_{j-l-1,k},\ldots,\mathbf{u}^n_{j+l,k})$. The case for the fluxes in the y-direction is equivalent running the k index instead of j.

Consistent high order approximations in time can be achieved through Runge–Kutta type convex combinations of high order spatial approximations computed from expression (41), ([25]).

In particular, we have implemented this numerical scheme to achieve third order accuracy in space and time. As the reconstruction procedure in space we have used the third order accurate Power Piecewise Hyperbolic Method ([24]) which has a three point stencil, i.e. $l = 1$. For the integration in time we have utilized the third order accurate TVD Runge–Kutta time stepping procedure proposed in [25].

6. Numerical results

In this section we present a set of numerical experiments for the system of MHD equations in one and two spatial dimensions using the third order accurate entropy-fix upwind scheme proposed in the previous section.

The proposed numerical method is stable under a CFL restriction determined by

$$\Delta t = C\frac{\Delta x}{\max(|u|+c_f)} \tag{42}$$

for one-dimensional experiments and

$$\Delta t = \frac{C}{\frac{\max\left(|u|+c^x_f\right)}{\Delta x}+\frac{\max\left(|v|+c^y_f\right)}{\Delta y}} \tag{43}$$

for two-dimensional ones where C is 0.8 in our calculations and the maximums are taken over all computational cells.

6.1. Brio–Wu shock tube problem

We consider the one-dimensional Riemann problem consisting of a shock tube with two initial constant states, u_L and u_R

$$(\rho,u,v,w,B_x,B_y,B_z,P) = \begin{cases}(1,0,0,0,0.75,1,0,1); & x\leqslant 0,\\ (0.125,0,0,0,0.75,-1,0,0.1); & x>0,\end{cases}$$

with $\gamma = 2$. We solve the one-dimensional 8×8 MHD system for $x\in[-1,1]$ with $N = 800$ equally spaced grid points. We compute until time $t = 0.2$. This example was proposed by Brio and Wu in [5] to show the formation of a compound wave containing an intermediate shock which is attached by a slow rarefaction wave. The solution of this problem consists of a left-moving fast rarefaction wave, a slow compound wave, a contact discontinuity, a right-moving slow shock and a right-moving fast rarefaction wave. The change of sign of B_y is responsible for the formation of the compound wave.

Fig. 3 shows the density profile, the x- and y-components of the velocity, the y-component of the magnetic field and the pressure profiles at time 0.2 computed with our third order accurate entropy-fix upwind scheme.

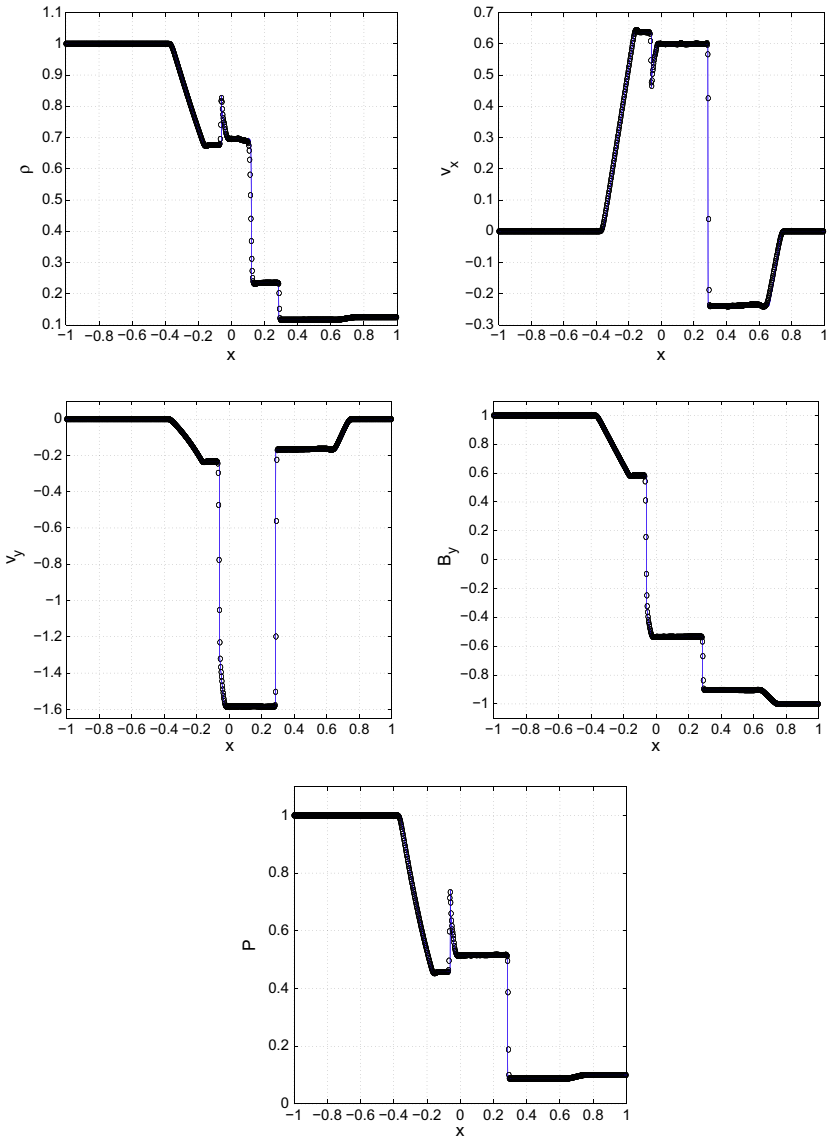

Fig. 3. Brio–Wu shock tube problem at time $t = 0.2$. Exact solution (solid line) versus computed approximation using the third order accurate entropy-fix upwind scheme with 800 grid points and $CFL = 0.8$: density profile (top left), x-component of the velocity (top right), y-component of the velocity (middle left), y-component of the magnetic field (middle right) and pressure (bottom).

Our scheme captures the complex features of the discontinuous MHD solution with high accuracy and low dissipation. The numerical results show that our scheme needs about four grid points to resolve shock layers and about six grid points to capture contact discontinuities. These numerical results are comparable to the calculations reported by Brio and Wu in [5] with a second order TVD scheme and the ones by Jiang and Wu in [15] with a fifth order accurate WENO Lax–Friedrichs scheme. Discontinuities by our scheme are resolved using the same number of grid points as the fifth order WENO scheme. Our third order approximation presents small oscillations near the trailing-edge of the right-moving fast rarefaction wave in the x-component of the velocity profile. These oscillations are of the order of the truncation error and less pronounced than the ones by the WENO scheme.

6.2. High Mach shock tube problem

The following shock tube problem is used to test the robustness of the numerical scheme for high Mach number flows. This Riemann problem consists of two constant states defined as

$$(\rho, u, v, w, B_x, B_y, B_z, P) = \begin{cases} (1,0,0,0,0,1,0,1000); & x \leqslant 0, \\ (0.125,0,0,0,0,-1,0,0.1); & x > 0, \end{cases}$$

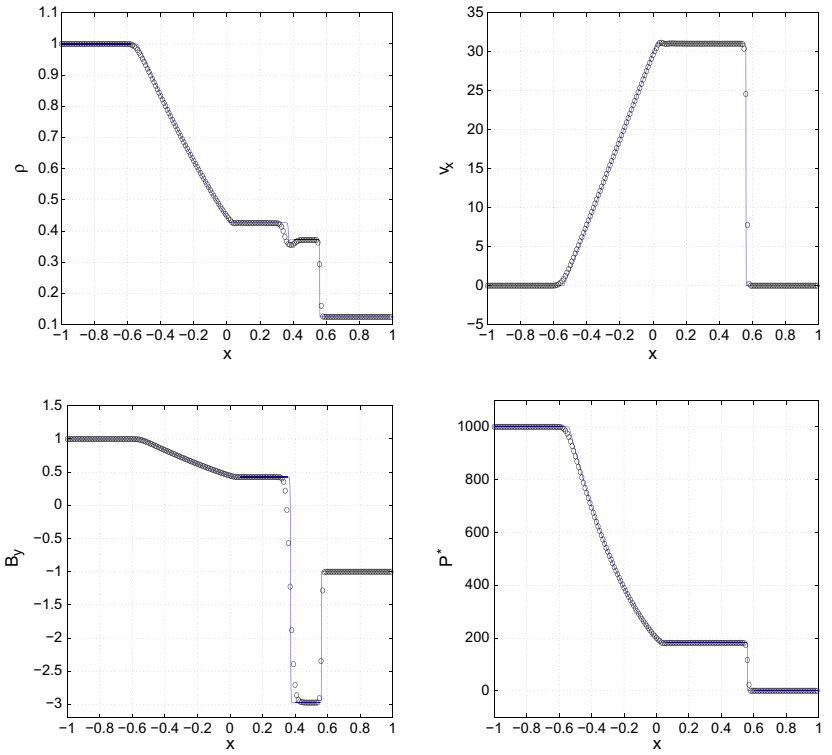

Fig. 4. High Mach shock tube problem at time $t = 0.012$. Exact solution (solid line) versus approximate solution computed by the third order accurate entropy-fix upwind scheme with 200 grid points and $CFL = 0.8$: density profile (top left), x-component of the velocity (top right), y-component of the magnetic field (bottom left) and the pressure (bottom right).

$x \in [-1, 1]$ and $\gamma = 2$. The resulting Mach number of the right-moving shock is 15.5. This problem becomes a standard gas dynamics Riemann problem if one replaces the hydrodynamic pressure by the sum of the plasma and the magnetic pressures. The solution of this problem consists of a left-moving fast rarefaction wave, a contact discontinuity (tangential one) and a right-moving fast shock. The total pressure and the fluid velocity are continuous through the contact wave although density, magnetic field and pressure may develop jumps. We perform the computation with 200 equally spaced grid points. The numerical approximation using our third order accurate entropy-fix upwind schemes is shown in Fig. 4 at $t = 0.012$ versus the exact solution (solid line). Note that the shocks appear very sharp and are resolved with two grid points without post-shock oscillations and the contact wave is approximated with six–seven grid points.

6.3. Orszag–Tang MHD turbulence problem

We consider the evolution of a compressible Orszag–Tang vortex system [7,19,21] using the two-dimensional MHD system of equations. The evolution of this complex flow contains many significant features of MHD turbulence involving inter-

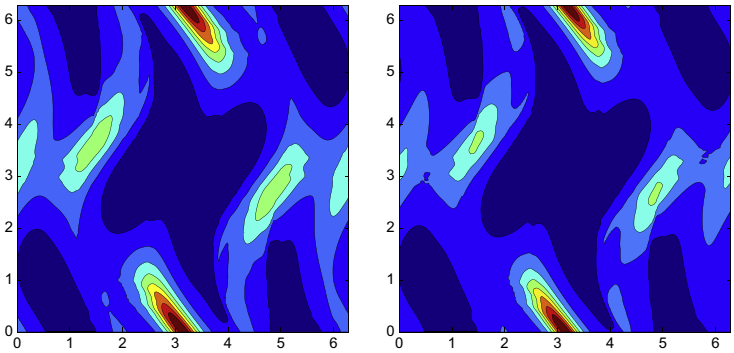

Fig. 5. Evolution of the compressible Orszag–Tang MHD turbulence problem at time $t = 0.5$. Numerical approximation of the density (left) and the pressure (right) computed by the third order accurate entropy-fix upwind scheme with 192×192 grid points.

actions between several shock waves traveling at different speeds and the formation of intermediate shocks. This vortex system was proposed as a test problem by Zachary et al. in [29] for the first time and has become a standard benchmark for MHD numerical schemes.

The initial data are given for $(x,y) \in [0,2\pi] \times [0,2\pi]$ by

$$\rho(x,y,0) = \gamma^2, \quad u(x,y,0) = -\sin(y), \quad v(x,y,0) = \sin(x),$$
$$p(x,y,0) = \gamma, \quad B_x(x,y,0) = -\sin(y), \quad B_y(x,y,0) = \sin(2x)$$

with $\gamma = 5/3$. Periodic boundary conditions are imposed in both x- and y-directions. We solve the MHD system with a uniform grid of 192×192 points using our third order accurate entropy-fix upwind scheme.

Figs. 5–7 show the numerical approximation of the Orszag–Tang vortex system at $t = 0.5, 2$ and $t = 3$, respectively.

The results are in excellent agreement with the ones in [2,15] and show the ability of our third order accurate entropy-fix upwind scheme to resolve shocks sharply and to capture fine structure of the vortex system.

6.4. Two dimension MHD Riemann problem

This Riemman problem consists of an initial data defined as constant states on each of the four quadrants of the domain. This problem was numerically studied in [23] for hydrodynamics and extended to MHD in [8] where an initial uniform magnetic field is introduced. We consider the four contacts Riemann problem defined in $x \in [-0.4, 0.4], y \in [-0.4, 0.4]$ by

$$(\rho, u, v, w, \mathbf{B}, P) = \begin{cases} (1, 0.75, -0.5, 0, \mathbf{B}, 1); & x \geqslant 0,\ y \geqslant 0 \\ (2, 0.75, 0.5, 0, \mathbf{B}, 1); & x < 0,\ y \geqslant 0 \\ (1, -0.75, 0.5, 0, \mathbf{B}, 1); & x < 0,\ y < 0 \\ (3, -0.75, -0.5, 0, \mathbf{B}, 1); & x \geqslant 0,\ y < 0 \end{cases}$$

where $\mathbf{B} = \frac{1}{\sqrt{8\pi}}(2,0,1)$ and $\gamma = 5/3$. We evolve until time $t = 0.8$ with 512×512 grid points and impose outflow boundary conditions. Fig. 8 displays the density and magnetic field profiles. The numerical results are in good agreement with those in [8].

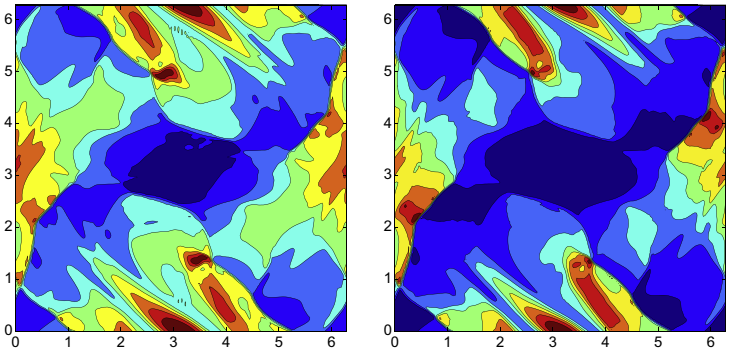

Fig. 6. Evolution of the compressible Orszag–Tang MHD turbulence problem at time $t = 2$. Numerical approximation of the density (left) and the pressure (right) computed by the third order accurate entropy-fix upwind scheme with 192×192 grid points.

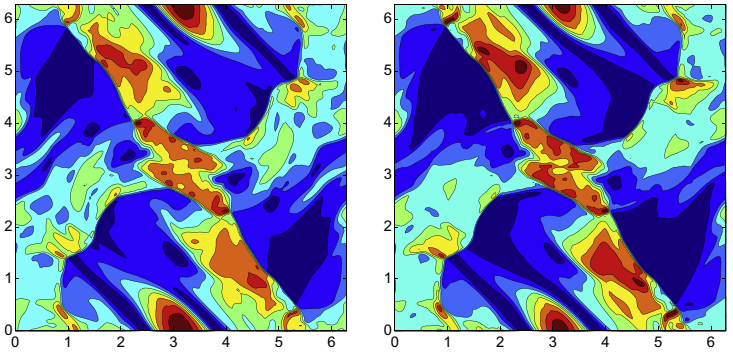

Fig. 7. Evolution of the compressible Orszag–Tang MHD turbulence problem at time $t = 3$. Numerical approximation of the density (left) and the pressure (right) computed by the third order accurate entropy-fix upwind scheme with 192×192 grid points.

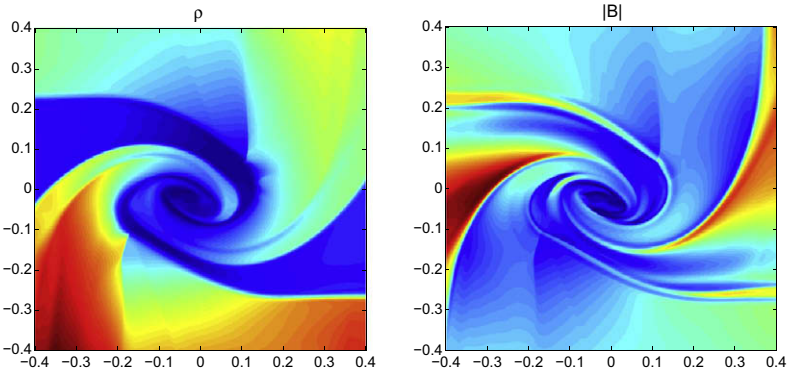

Fig. 8. Evolution at time $t = 0.8$ of the 2D Riemann problem. Left: mass density. Right: magnetic field $|B|$.

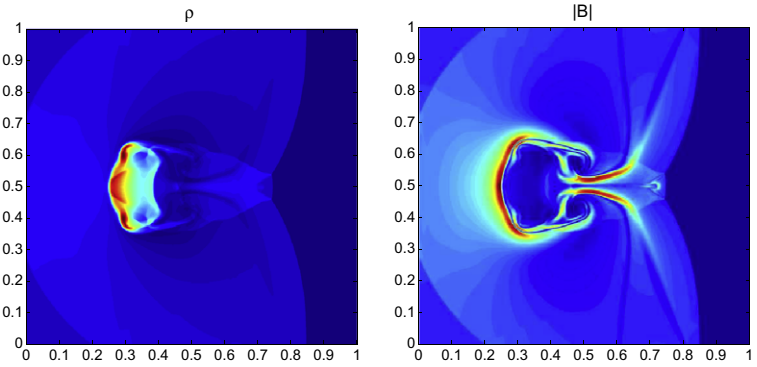

Fig. 9. Evolution of a magnetosonic shock interacting with a high-density cloud computed with a 512×512 grid at time $t = 0.06$. Density (left) and magnetic field $|B|$ (right).

6.5. Interaction between a strong shock and a high-density cloud

This two-dimensional MHD problem was proposed in [8] and describes the interaction between a Mach 10 shock wave and a high-density cloud. The initial conditions of the problem for the two states separated by a discontinuity at $x = 0.6$ are given for $x \in [0,1], y \in [0,1]$ by

$$(\rho, u, v, w, B_x, B_y, B_z, P) = \begin{cases} (3.86859, 0, 0, 0, 0, -2.1826182, 2.1826182, 167.34); & x < 0.6, \\ (1, -11.2536, 0, 0, 0, 0.56418958, 0.56418958, 1); & x > 0.6. \end{cases}$$

The circular cloud of radius 0.15 is centered at $(x, y) = (0.8, 0.5)$ and has a density $\rho = 10$. In Fig. 9 we display the density and magnetic field profiles computed with 512×512 grid points, $\gamma = 5/3$ at time $t = 0.06$ imposing outflow boundary conditions. The numerical results show the ability of our entropy-fix upwind scheme to resolve highly supersonic MHD flows.

The numerical experiments tested in this section demonstrate good behavior of our scheme. The performance of the numerical scheme is stable and robust for different values of the adiabatic exponent γ. The results show that the choice of a low dissipative scheme with an appropriate entropy correction allows to resolve discontinuities sharply and to capture fine scales avoiding the use of a very high order accurate version of the scheme.

7. Conclusions

We have performed an analysis of the wave structure of the ideal MHD equations. We have presented a complete system of eigenvectors of the Jacobians of the fluxes that allows to derive an analytical expression of the nonlinearity term associated to each characteristic field. We have deduced a criterion for the detection of local regions containing points for which a nonlinear characteristic field becomes nonconvex. We have designed a characteristic-based upwind scheme for the ideal MHD equations that resolves the wave dynamics by local characteristic wavefields using the proposed complete system of eigenvectors. The new scheme is able to detect local regions containing nonconvexity points and to handle an entropy correction by prescribing a local viscosity ensuring convergence to the entropy solution. A third order accurate version of the scheme performs satisfactorily in resolving one and two-dimensional MHD problems.

References

[1] J. Balbás, E. Tadmor, C.C. Wu, Non-oscillatory central schemes for one- and two-dimensional MHD equations: I, J. Comput. Phys. 201 (2004) 261–285.
[2] J. Balbás, E. Tadmor, Nonoscillatory central schemes for one- and two-dimensional magnetohydrodynamics equations. II: High-order semidiscrete schemes, SIAM J. Sci. Comput. 28 (2) (2006) 533–560.
[3] J.U. Brackbill, J.C. Barnes, The effect of nonzero div *B* on the numerical solution of the magnetohydrodynamic equations, J. Comput. Phys. 35 (1980) 426.
[4] M. Brio, C.C. Wu, Characteristic fields for the equations of magnetohydrodynamics, nonstrictly hyperbolic conservation laws, Contemp. Math. 60 (1985) 19–24.
[5] M. Brio, C.C. Wu, An upwind differencing scheme for the equations of ideal magnetohydrodynamics, J. Comput. Phys. 75 (2) (1988) 400–422.
[6] R. Courant, K.O. Friedrichs, Supersonic Flow and Shock Waves, Springer, New York, 1999.
[7] R.B. Dahlburg, J.M. Picone, Evolution of the Orszag–Tang vortex system in a compressible medium I. Initial average subsonic flow, Phys. Fluids B 1 (1989) 2153–2171.
[8] W. Dai, P.R. Woodward, A simple finite difference scheme for multidimensional magnetohydrodynamical equations, J. Comput. Phys. 142 (2) (1998) 331–369.
[9] R. Donat, A. Marquina, Capturing shock reflections: an improved flux formula, J. Comput. Phys. 125 (1996) 42–58.
[10] C.R. Evans, J.F. Hawley, Simulation of magnetohydrodynamic flows – a constrained transport method, Astrophys. J. 332 (1988) 659–677.
[11] S.K. Godunov, Difference methods for the numerical calculation of the equations of fluid dynamics, Math. Sbornik 47 (1959) 271–306.
[12] I.M. Gelfand, Some problems in the theory of quasilinear equations, Am. Math. Soc. Trans. 29 (2) (1963) 295–381.
[13] A. Harten, B. Enquist, S. Osher, S.R. Chakravarthy, Uniformly high order accurate essentially non-oscillatory schemes III, J. Comput. Phys. 71 (1987) 231–303.
[14] A. Jeffrey, T. Taniuti, Nonlinear Wave Propagation, Academic Press, New York, 1964.
[15] G.S. Jiang, C.C. Wu, A high-order WENO finite difference scheme for the equations of ideal magnetohydrodynamics, J. Comput. Phys. 150 (2) (1999) 561–594.
[16] P.D. Lax, Hyperbolic systems of conservation laws 2, Commun. Pure Appl. Math. 10 (4) (1957) 537–566.
[17] P.D. Lax, Hyperbolic systems of conservation laws and the mathematical theory of shocks waves SIAM, Philadelphia, 1973.
[18] S.T. Li, An HLLC Riemann solver for magneto-hydrodynamics, J. Comput. Phys. 203 (1) (2005) 344–357.
[19] S.A. Orszag, C.M. Tang, Small scale structure of two-dimensional magnetohydrodynamic turbulence, J. Fluid Mech. 90 (1979) 129–143.
[20] J.M. Picone, R.B. Dahlburg, Evolution of the Orszag–Tang vortex system in a compressible medium II. Supersonic flow, Phys. Fluids B 3 (1991) 29–44.
[21] K.G. Powell, P.L. Roe, R.S. Myong, T. Gombosi, D. deZeeuw, An upwind scheme for magnetohydrodynamics, AIAA 12th Computational Fluid Dynamics Conference, San Diego, CA, 1995, pp. 661–674.
[22] P.L. Roe, Approximate Riemann solvers, parameter vectors, and difference schemes, J. Comput. Phys. 43 (2) (1981) 357–372.
[23] C.W. Schulz-Rinne, J.P. Collins, H.M. Glaz, Numerical solution of the Riemann problem for two-dimensional gas dynamics, SIAM J. Sci. Comput. 14 (1993) 1394–1414.
[24] S. Serna, A class of extended limiters applied to Piecewise Hyperbolic methods, SIAM J. Sci. Comput. 28 (1) (2006) 123–140.
[25] C.W. Shu, S. Osher, Efficient implementation of essentially non-oscillatory shock-capturing schemes 2, J. Comput. Phys. 83 (1) (1989) 32–78.
[26] G. Toth, The $\nabla B = 0$ constraint in shock-capturing magnetohydrodynamics codes, J. Comput. Phys. 161 (2000) 605–652.
[27] C.C. Wu, Formation, structure and stability of MHD intermediate shocks, J. Geophys. Res. 95 (1990) 8149–8175.
[28] C.C. Wu, Magnetohydrodynamic Riemann problem and the structure of the magnetic reconnection layer, J. Geophys. Res. 100 (1995) 5579–5598.
[29] A.L. Zachary, A. Malagoli, P. Colella, A higher-order Godunov method for multidimensional magnetohydrodynamics, SIAM J. Sci. Comput. 15 (1994) 263–284.